an angle of attack of 8 deg the pattern is similar to that at $\alpha = 4$ deg, that is, the "cold streak" along the centerline is still present. At angles of attack of 12 and 16 deg the forebody windward heating is similar to that which occurs on a delta wing at high angle of attack.[3]

Figure 2 is a comparison of data and theory on the fuselage bottom at an angle of attack of 8 deg, along a data line which passes through the turbulent area. The theories shown utilize the T' method for laminar heating and the Spaulding-Chi method as modified by Neal and Bertram[4] for turbulent values. The Hypersonic Arbitrary Body Program,[5] modified to provide the heat transfer information, generated the boundary layer edge conditions using the tangent cone approximation. The turbulent heating theory has been shifted by assuming that the end of transition was equivalent to a new sharp leading edge or virtual origin. This location was determined from the earliest melt (or highest heating) of the region assumed to be turbulent. As shown in Fig. 2, the two theories bracket the data and the turbulent theory starting from a virtual origin location of $X/L = 0.3$ gives good agreement with the data.

Leeside Heating

A sequence of phase-change patterns on the leeside at an angle of attack of 4 deg is shown in Fig. 3. The first photograph of the sequence shows transition from laminar to fully turbulent flow on the wing and melted regions (high heating rates) on the canopy and leading edges. In the second photograph, melt is occurring on the sides along a line just inboard of the fuselage leading edge (note that the heating level here is comparable to that on the canopy and the leading edges). The third photograph indicates the extent of the high heating rates on the sides along with the interference heating downstream of the canopy, at the wing root, center-vertical tail/fuselage juncture and upstream of the drag brakes, as well as the leading-edge heating upstream of the canopy. The salient feature in the final photograph is the interference heating along the leeward centerline produced by the vortex which begins aft of the canopy.

The data along the fuselage side are compared with theory in Fig. 4 for $\alpha = 8$ deg. Again, the agreement between data and the prediction method is reasonably good.

Concluding Remarks

The Hypersonic Arbitrary Body Program (HABP) in conjunction with accepted, easily used heat-transfer prediction techniques has been shown to give reasonably good overall agreement with experimental results and is a reasonable way to predict the type of heating information needed to generate nominal thermal protection system weights. The phase-change paint technique gives easily interpreted graphic indication of local areas not covered by assumptions of the analytic technique along with the heating level to allow detail corrections to the thermal protection system. The paint technique also allows a rapid check of the heating level over the large areas of the test model.

References

[1] Kirkham, F.S. and Jones, R.A., "Joint USAF/NASA Hypersonic Research Aircraft Study," AIAA Paper 75-1039, Anaheim, Calif., Aug. 1975.

[2] Jones, R.A. and Hunt, J.L., "Use of Fusible Temperature Indicators for Obtaining Quantitative Aerodynamic Heat-Transfer Data," NASA TR R-230, Feb. 1966.

[3] Johnson, C.B. "Boundary-Layer Transition and Heating Criteria Applicable to Space Shuttle Configurations from Flight and Ground Tests," presented at NASA Space Shuttle Technology Conference; Volume I—Aerothermodynamics, Configurations, and Flight Mechanics," NASA TM X-2272, April 1971.

[4] Neal, L., Jr. and Bertram, M.H., "Turbulent-Skin-Friction and Heat-Transfer Charts Adapted from the Spaulding-Chi Method," NASA TN D-3969, 1967.

[5] Gentry, A.E. and Smyth, D.C., "Hypersonic Arbitrary-Body Aerodynamic Component Program (Mark III Version)," Vol. II—Program Formulation and Listings," Rep. DAC 61552, Vol. II—(Air Force Contract Nos. F3361 67 C 1008 and F33615 67 C 1602), McDonnell Douglas Corporation, April 1968 (available from DDC as 851 812).

Aerodynamics of Sideslipping Delta Wings at Incidence with Leading-Edge Separation

M.J. Cohen*
The Technion, Israel Institute of Technology, Haifa, Israel

Nomenclature

p = rolling speed, $\bar{p} = ps/V\epsilon$
s = local semispan of delta wing
s_o = local semispan of delta wing at pitch axis, $\bar{s_o} = s_o/s$
U = relative wind velocity
x,y = coordinates in Z-plane, $Z = x + iy$
$\bar{Z}$ = Z/s, $\bar{Z} = \frac{1}{2}(\xi + 1/\xi)$
C_p = pressure coefficient, $C_p = p/(\frac{1}{2}\rho U^2)$
C_L = normal force coefficient, $C_L = L/(\frac{1}{2}\rho U^2 S)$
C_l = rolling moment coefficient about body axis in the plane of symmetry of the wing, $C_l = \ell/(\frac{1}{2}\rho U^2 Ss)$
α = angle of incidence, $\bar{\alpha} = \alpha/\epsilon$
β = angle of sideslip, $\bar{\beta} = \beta/\epsilon$
Γ_i = vortex core strength
ϵ = semiapex angle of delta wing
θ = polar angle defined by $y = s\cos\theta$
ρ,σ = polar coordinates of a point in the ξ-plane, $\xi = \rho e^{i\sigma}$
σ_i = angular location of vortex cores in the ξ-plane,
ξ = $\rho e^{i\sigma}$, $\bar{\xi} = 2\xi/s = \bar{\rho} e^{i\sigma}$, $\bar{\xi} = \bar{Z} + (\bar{Z}^2 - 1)^{\frac{1}{2}}$
i = 1,2: subscripts relating quantities to windward and leeward isolated vortices, respectively

Introduction

UPON consideration of previous work by D. Nimri and the author,[1] it became evident that the solution of the problem of the slender delta wing in sideslip and in separated flow could be obtained as a derivative of the more general solution presented in that reference. The desirability of describing here that special solution was reinforced by the then lack of existing theoretical work on the subject, coupled with the realization that it would afford a useful, approximate, closed-form solution to a problem of practical concern. It was only after this task was accomplished that the author became aware that Pullin[2] had recently obtained numerically developed solutions for the same problem. In view of the simplicity of the closed-form expressions for the aerodynamic coefficients which are derived in the sequel, it has been decided to present these nonetheless and to test some of the results against (1) Pullin's results in the practical parametral $(\bar{\alpha},\bar{\beta})$ range, and (2) Harvey's[3] experimental data for specific wings operating under conditions covered by both methods. Furthermore, the range of applicability of the present method includes the low-incidence $(\bar{\alpha} \leq 0.5)$ subrange, in parts of which $(\bar{\beta} \geq 1.0)$ Pullin's numerical procedure fails to yield a solution.

Received Feb. 2, 1976; revision received May 26, 1976.
Index category: Aircraft Aerodynamics (including Component Aerodynamics).

*Associate Professor, Department of Aeronautics. Member AIAA.

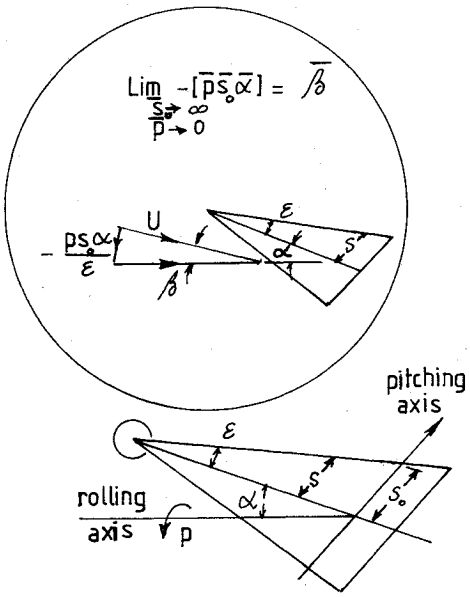

Fig. 1 Wing geometry.

Theoretical Background

The potential flow model of a sideslipping delta wing at incidence with leading-edge separation is, to slender body theory approximation, conical. Consider (Fig. 1) the geometry of the rolling delta wing at incidence. In that figure a microregion near the apex is shown suitably magnified. It is clear that the flow past a sideslipping wing corresponds to that in the microregion in the limiting case of a rolling wing as $\bar{p}\to 0$, $\bar{s}_o\to\infty$ with s remaining finite, since then

$$-\bar{p}\bar{s}_o\bar{\alpha}=\bar{\beta} \tag{1}$$

The two conditions for smooth outflow at the leading edges as $\bar{p}\to 0$ becomes[1]

$$\frac{\bar{\Gamma}_1(\bar{\rho}_1^2-1)}{\bar{\rho}_1^2+1-2\cos\sigma_1}+\frac{\bar{\Gamma}_2(\bar{\rho}_2^2-1)}{\bar{\rho}_2^2+1+2\cos\sigma_2}=-\bar{\alpha}$$

$$\frac{\bar{\Gamma}_2(\bar{\rho}_2^2-1)}{\bar{\rho}_2^2+1-2\cos\sigma_2}+\frac{\bar{\Gamma}_1(\bar{\rho}_1^2-1)}{\bar{\rho}_1^2+1+2\cos\sigma_1}=+\bar{\alpha} \tag{2}$$

The condition of zero net force on each combined vortex core and feeding vortex trace, representing each of the windward and leeward shed vortex systems, yields, using Eq.

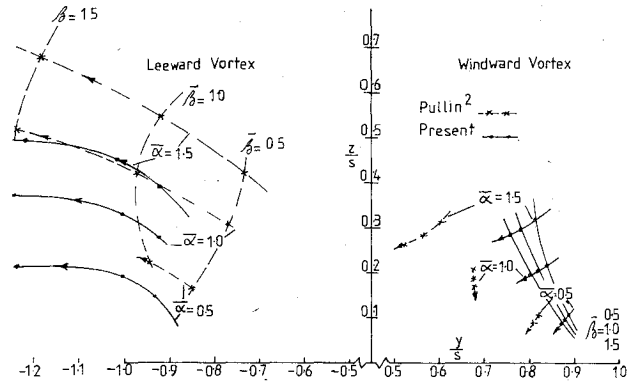

Fig. 2 Vortex core position.

(1), the limiting forms of two complex equations[1] (for the conical flow considered here, $n=1$), namely

$$i\{(2\bar{\bar{Z}}_1-1)+\bar{\beta}\}=\frac{\bar{\xi}_1^2+1}{\bar{\xi}_1^2-1}\cdot\bar{\alpha}-\frac{2\bar{\xi}_1^2}{\bar{\xi}_1^2-1}$$

$$\times\left\{\frac{-\bar{\rho}_1^2\bar{\Gamma}_1}{(\bar{\rho}_1^2-1)\bar{\xi}_1}-\frac{\bar{\Gamma}_1}{(\bar{\xi}_1^2-1)\bar{\xi}_1}+\frac{\bar{\Gamma}_2\bar{\xi}_2(\bar{\rho}_2^2-1)}{(\bar{\xi}_1-\bar{\xi}_2)(\bar{\rho}_2^2\bar{\xi}_1-\bar{\xi}_2)}\right\}$$

$$i\{(2\bar{\bar{Z}}_2+1)+\bar{\beta}\}=\frac{\bar{\xi}_2^2+1}{\bar{\xi}_2^2-1}\cdot\bar{\alpha}-\frac{2\bar{\xi}_2^2}{\bar{\xi}_2^2-1}$$

$$\times\left\{\frac{-\bar{\rho}_2^2\bar{\Gamma}_2}{(\bar{\rho}_2^2-1)\bar{\xi}_2}-\frac{\bar{\Gamma}_2}{(\bar{\xi}_2^2-1)\bar{\xi}_2}+\frac{\bar{\Gamma}_1\bar{\xi}_1(\bar{\rho}_1^2-1)}{(\bar{\xi}_2-\bar{\xi}_1)(\bar{\rho}_1^2\bar{\xi}_2-\bar{\xi}_1)}\right\} \tag{3}$$

where $\bar{\xi}_1=\bar{\rho}_1e^{i\sigma 1}$, $\bar{\xi}_2=\bar{\rho}_2e^{i\sigma 2}$, and $\bar{Z}$ is the conjugate of $\bar{Z}$. In Eq. (3) $\bar{Z}$ and $\bar{\xi}$ are linked by the transformation relation,[1]

$$\bar{Z}=\tfrac{1}{2}(\bar{\xi}+1/\bar{\xi}) \tag{4}$$

Equations (2) and (3) form a system of six nonlinear simultaneous equations for the determination of the six unknowns $(\bar{\Gamma}_1,\bar{\rho}_1,\sigma_1)$ and $(\bar{\Gamma}_2,\bar{\rho}_2,\sigma_2)$. They have been solved using an optimum descent technique for a representative range of the control parameters $\bar{\alpha}$ and $\bar{\beta}$ and the results will be found tabulated in Table 1. The vortex core locations are plotted in Fig. 2. The limiting form of the pressure coefficient

Table 1 Results

	Windward vortex					Leeward vortex				
	$-\bar{\Gamma}_1$	$\bar{\rho}_1$	σ_1	x_1	y_1	$\bar{\Gamma}_2$	$\bar{\rho}_2$	σ_2	$-x_2$	y_2
$\bar{\alpha}=0.5$										
$\bar{\beta}=0.5$	0.397	1.233	.519	.888	.105	0.280	1.369	2.658	0.930	.149
1.0	0.450	1.205	.526	.880	.094	0.219	1.594	2.730	1.018	.193
1.5	0.516	1.189	.536	.873	.089	0.217	2.098	2.878	1.243	.211
$\bar{\alpha}=1.0$										
$\bar{\beta}=0.5$	0.904	1.409	.659	.838	.214	0.688	1.614	2.540	0.921	.281
1.0	1.014	1.362	.674	.818	.196	0.595	1.861	2.613	1.036	.334
1.5	1.140	1.330	.689	.804	.185	0.570	2.278	2.727	1.244	.370
$\bar{\alpha}=1.5$										
$\bar{\beta}=0.5$	1.490	1.566	.745	.810	.315	1.196	1.809	2.466	0.922	.393
1.0	1.657	1.508	.769	.780	.294	1.082	2.063	2.535	1.047	.450
1.5	1.847	1.470	.790	.756	.281	1.040	2.448	2.631	1.246	.498
$\bar{\alpha}=2.0$										
$\bar{\beta}=0.5$	2.140	1.700	.802	.795	.400	1.780	1.960	2.416	0.924	.482
1.0	2.307	1.638	.832	.757	.380	1.651	2.218	2.480	1.053	.549
1.5	2.610	1.598	.860	.725	.369	1.602	2.588	2.560	1.247	.600

using condition (1) yields[1]

$$\frac{C_p}{\epsilon^2} = -2\left\{\bar{\alpha}\sec\theta + \frac{\bar{\Gamma}_1(\bar{\rho}_1^2-1)}{\bar{\rho}_1^2+1-2\bar{\rho}_1\cos(\theta-\sigma_1)} + \frac{\bar{\Gamma}_2(\bar{\rho}_2^2-1)}{\bar{\rho}_2^2+1-2\bar{\rho}_2\cos(\theta-\sigma_2)}\right\}\cot\theta$$

$$-\left\{\bar{\alpha}\cos\theta+\bar{\beta}\sin\theta + \frac{\bar{\Gamma}_1(\bar{\rho}_1^2-1)}{\bar{\rho}_1^2+1-2\bar{\rho}_1\cos(\theta-\sigma_1)} + \frac{\bar{\Gamma}_2(\bar{\rho}_2^2-1)}{\bar{\rho}_2^2+1-2\bar{\rho}_2\cos(\theta-\sigma_2)}\right\}^2 \csc^2\theta+\bar{\alpha}^2+\bar{\beta}^2 \quad (5)$$

With $(\bar{\Gamma}_1,\bar{\rho}_1,\sigma_1)$, $(\bar{\Gamma}_2,\bar{\rho}_2,\sigma_2)$ now known for given operational values of $\bar{\alpha}$ and $\bar{\beta}$, C_p/ϵ^2 can be evaluated for any case.

Normal Force and Rolling Moment Coefficients

For any operational pair $(\bar{\alpha},\bar{\beta})$ the normal coefficient C_L is still given by[1]

$$\frac{C_L}{\epsilon^2} = 2\pi\bar{\alpha}\left\{1-\left[\frac{\bar{\Gamma}_1(\bar{\alpha}_1\bar{\beta})}{\bar{\alpha}}(\bar{\rho}_1-1/\bar{\rho}_1)\cos\sigma_1 + \frac{\bar{\Gamma}_2(\bar{\alpha}_1\bar{\beta})}{\bar{\alpha}}(\bar{\rho}_2-1/\bar{\rho}_2)\cos\sigma_2\right]\right\} \quad (6)$$

where the two sets $(\bar{\Gamma}_1,\bar{\rho}_1,\sigma_1)$ and $(\bar{\Gamma}_2,\bar{\rho}_2,\sigma_2)$ required for the evaluation of C_L can be obtained from Table 1 for the given values of the pair $(\bar{\alpha},\bar{\beta})$. The rolling moment coefficient in separated flow, about a rolling axis in the plane of symmetry of the sideslipping wing, is given by a modified form of expression (23) of Ref. 1, namely, by

$$\frac{C_l}{\epsilon^2} = -\frac{\pi}{3}\bar{\beta}\{\bar{\alpha}-[\bar{\Gamma}_1(\bar{\alpha}_1\bar{\beta})(\bar{\rho}_1-1/\bar{\rho}_1)\cos\sigma_1 + \bar{\Gamma}_2(\bar{\alpha},\bar{\beta})(\bar{\rho}_2-1/\bar{\rho}_2)\cos\sigma_2]\} + \frac{\pi}{2}\{\bar{\Gamma}_1(\bar{\alpha},\bar{\beta})[2|\bar{Z}_1|^2-\tfrac{1}{2}(1/\bar{\xi}_1^2+1/\bar{\xi}_1^2+2)] + \bar{\Gamma}_2(\bar{\alpha},\bar{\beta})[2|\bar{Z}_2|^2-\tfrac{1}{2}(1/\bar{\xi}_2^2+1/\bar{\xi}_2^2+2)]\} \quad (7)$$

Equations (6) and (7) are closed-form expressions for C_L and C_l for a slender delta wing at incidence and in sideslip with leading edge separation. These functions have been calculated in the range $0\le\bar{\alpha}\le 1.5$, $0\le\bar{\beta}\le 1.5$, and their parametral dependence in that range is plotted in Figs. 3 and 4.

Results and Conclusions

Figure 2 shows the shift in the positions of the vortex cores as the sideslip angle increases for three values of the incidence $\bar{\alpha}=0.5$, 1.0, 1.5. The windward vortex moves "in" and "down" towards the wing, whereas the leeward vortex moves "out" and "up" from the wing. This tendency also shows up in Pullin's work which, however, yields isolated core vortices positioned more inboard for both leeward and windward systems, in greater accord with Harvey's[3] results. The vortex strengths $\bar{\Gamma}_i$ given by the present model are, on the other hand, practically identical to the combined sheet vorticity and isolated vortex strengths of the windward and leeward shed vorticity systems used by Pullin.

Figure 3 shows the variation of the normal force in the presence of both incidence and sideslip. Both Pullin's results, where available, and those derived by the present method give excellent agreement with experiment[3] at the lower incidences $\bar{\alpha}\le 0.5$. For $\alpha\ge 1.0$ the present method appears to increasingly overestimate and Pullin's possibly to increasingly underestimate the actual normal force acting on the wing as

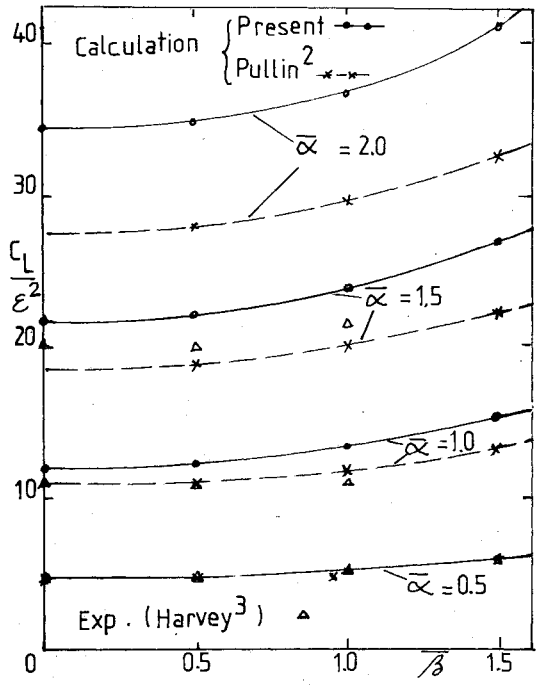

Fig. 3 Normal force coefficient.

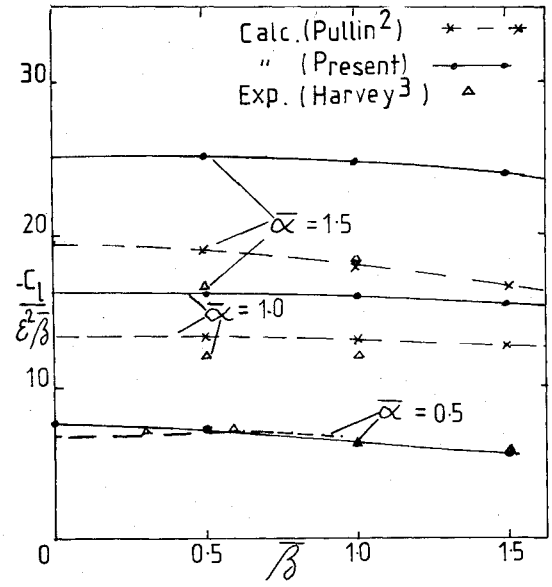

Fig. 4 Rolling moment coefficient.

the incidence increases. Nonetheless, in that subrange Pullin's results are closer to the experimental values where available.

Figure 4 exhibits the rolling moment coefficient's $C_l/\epsilon^2\bar{\beta}$ dependence on sideslip in separated flow in the range $0.5\le\bar{\alpha}\le 1.5$. Once again, at relatively low incidences $\bar{\alpha}\le 0.5$, the method presented here gives very good agreement with experiment throughout the sideslip range. At the higher incidences, however, ($\bar{\alpha}\ge 1.0$) both Pullin's and the present method appear to increasingly overestimate this rolling moment due to sideslip in detached flow, with the former, however, consistently given better concordance with experimentally measured values.[3]

References

[1] Cohen, M.J. and Nimri, D., "Aerodynamics of Rolling Slender Wings at Incidence in Separated Flow," *AIAA Journal*, (to be published.

[2] Pullin, D.I., "Calculations of the Steady Conical Flow Past a Yawed Slender Delta Wing with Leading Edge Separation," ARC R&M 3767, 1975.

[3] Harvey, J.K., "Some Measurements on a Yawed Slender Wing with Leading Edge Separation." ARC R&M 3160, 1958.